Radiology

Acute Microstructural Changes after ST-Segment Elevation Myocardial Infarction Assessed with Diffusion Tensor Imaging

Arka Das, MBChB • Christopher Kelly, PhD • Irvin Teh, PhD • Christian T. Stoeck, PhD • Sebastian Kozerke, PhD • Amrit Chowdhary, MBBS • Louise A. E. Brown, MBChB • Christopher E. D. Saunderson, MD • Thomas P. Craven, MBBS • Pei G. Cheu, MD • Nicholas Jex, MBBS • Peter P. Swoboda, PhD • Eylem Levelt, DPhil • John P. Greenwood, PhD • Jurgen E. Schneider, PhD • Sven Plein, PhD • Erica Dall'Armellina, DPhil

From the Biomedical Imaging Science Department, Leeds Institute of Cardiovascular and Metabolic Medicine, University of Leeds, and Leeds Teaching Hospitals NHS Trust, Clarendon, Way, Leeds LS2 9JT, England (A.D., C.K., I.T., A.C., L.A.E.B., C.E.D.S., T.P.C., P.G.C., N.J., P.P.S., E.L., J.P.G., J.E.S., S.P., E.D.); and Institute for Biomedical Engineering, University and ETH Zurich, Zurich, Switzerland (C.T.S., S.K.). Received July 24, 2020; revision requested August 20; revision received November 20; accepted December 3. **Address correspondence to** E.D. (e-mail: *E.DallArmellina@leeds.ac.uk*).

A.D. supported by Heart Research UK (grant no. RG2668/18/20). C.T.S. supported by the Swiss National Science Foundation (grant no. PZ00P2_174144). S.P. supported by a British Heart Foundation Chair (grant no. CH/16/2/32089). E.D. is a British Heart Foundation Intermediate Clinical Research Fellow (grant no. FS/13/71/30378).

Conflicts of interest are listed at the end of this article.

Radiology 2021; 299:86–96 • https://doi.org/10.1148/radiol.2021203208 • Content codes: CA MR

Background: Cardiac diffusion tensor imaging (cDTI) allows for in vivo characterization of myocardial microstructure. In cDTI, mean diffusivity and fractional anisotropy (FA)—markers of magnitude and anisotropy of diffusion of water molecules—are known to change after myocardial infarction. However, little is known about regional changes in helix angle (HA) and secondary eigenvector angle (E2A), which reflects orientations of laminar sheetlets, and their association with long-term recovery of left ventricular ejection fraction (LVEF).

Purpose: To assess serial changes in cDTI biomarkers in participants following ST-segment elevation myocardial infarction (STEMI) and to determine their associations with long-term left ventricular remodeling.

Materials and Methods: In this prospective study, 30 participants underwent cardiac MRI (3 T) after STEMI at 5 days and 3 months after reperfusion (National Institute of Health Research study no. 33963 and Research Ethics no. REC17/YH/0062). Spin-echo cDTI with second-order motion-compensation (approximate duration, 13 minutes; three sections; 18 noncollinear diffusion-weighted scans with b values of 100 sec/mm^2 [three acquisitions], 200 sec/mm^2 [three acquisitions], and 500 sec/mm^2 [12 acquisitions]), functional images, and late gadolinium enhancement images were obtained. Multiple regression analysis was used to assess associations between acute cDTI parameters and 3-month LVEF.

Results: Acutely infarcted myocardium had reduced FA, E2A, and myocytes with right-handed orientation (RHM) on HA maps compared with remote myocardium (mean remote FA = 0.36 ± 0.02 [standard deviation], mean infarcted FA = 0.25 ± 0.03, $P <$ .001; mean remote E2A = 55° ± 9, mean infarcted E2A = 49° ± 10, $P <$ .001; mean remote RHM = 16% ± 6, mean infarcted RHM = 9% ± 5, $P <$ .001). All three parameters (FA, E2A, and RHM) correlated with 3-month LVEF (r = 0.68, r = 0.59, and r = 0.53, respectively), with acute FA being independently predictive of 3-month LVEF (standardized β = 0.56, P = .008) after multivariable analysis adjusting for factors, including acute LVEF and infarct size.

Conclusion: After ST-segment elevation myocardial infarction, diffusion becomes more isotropic in acutely infarcted myocardium as reflected by decreased fractional anisotropy. Reductions in secondary eigenvector angle suggest that the myocardial sheetlets are unable to adopt their usual steep orientations in systole, whereas reductions in myocytes with right-handed orientation on helix angle maps are likely reflective of a loss of organization among subendocardial myocytes. Correlations between these parameters and 3-month left ventricular ejection fraction highlight the potential clinical use of cardiac diffusion tensor imaging after myocardial infarction in predicting long-term remodeling.

Online supplemental material is available for this article.

Left ventricular (LV) remodeling after myocardial infarction is characterized by chamber dilatation and regional wall thinning. The disproportionate increase in myocyte length, without the adaptive increase in myocyte cross-sectional area that is needed for force generation, leaves the long slender myocytes at a mechanical disadvantage during the ensuing increasing wall stress and leads to worsening functional impairment over time (1). In healthy myocardium, cardiomyocytes aggregate together to form laminar secondary structures known as sheetlets. Reorientation of sheetlets throughout the cardiac cycle is thought to be the principal mechanism driving LV wall thickening during systole (2); however, the impact of ischemic injury on sheetlets has not been explored in detail. Despite the range of techniques that cardiac MRI helps provide for quantifying myocardial edema, scarring, and the consequent impairment in myocardial deformation and contractility after myocardial infarction, current techniques do not allow for the assessment of the organization and integrity of microstructural components. However, with the emergence of

Abbreviations

cDTI = cardiac diffusion tensor imaging, ECV = extracellular volume, E2A = secondary eigenvector angle, FA = fractional anisotropy, HA = helix angle, LGE = late gadolinium enhancement, LV = left ventricle, LVEF = left ventricular ejection fraction, MD = mean diffusivity, MVO = microvascular obstruction, RHM = myocytes with right-handed orientation, STEMI = ST-segment elevation myocardial infarction

Summary

Cardiac diffusion tensor imaging can be used to detect early and irreversible myocardial microstructural remodeling that may improve the prediction of left ventricular functional recovery at 3 months.

Key Results

- Acutely infarcted myocardium had lower fractional anisotropy (FA) (remote FA = 0.36, infarcted FA = 0.25; $P < .001$), lower secondary eigenvector angle (E2A) (remote E2A = 55°, infarcted E2A = 49°; $P < .001$), and reduced proportions of right-handed myocytes (RHM) corresponding to subendocardium (remote RHM = 16%, infarcted RHM = 9%; $P < .001$) than remote myocardium.
- Acutely infarcted FA, E2A, and RHM correlate with left ventricular ejection fraction at 3 months ($r = 0.68$, $r = 0.59$, and $r = 0.53$, respectively), with acute FA being an independent predictor after multivariable linear regression analysis (standardized $\beta = 0.56$, $P = .008$).

cardiac diffusion tensor imaging (cDTI), this has now become possible (3,4).

Based on the principle that water diffusion occurs preferentially along the long axis of cardiomyocytes, cDTI can provide information about the predominant orientations of cardiomyocytes and sheetlets within the myocardium (5). Previous cDTI studies on animal (6–8) and human (9–13) hearts have shown an increase in mean diffusivity (MD) and a decrease in the anisotropy of diffusion of water molecules defined by fractional anisotropy (FA) (Fig 1, *A* and *B*) immediately after myocardial infarction. Based on histologic corroboration, the proposed mechanisms for these changes include the concomitant effects of edema, expansion in extracellular space, cardiomyocyte disarray, and collagen infiltration (6). The longitudinal changes in MD and FA remain an area of interest (13).

In cDTI, the secondary eigenvector angle (E2A) is a proposed measurement of the orientation of laminar sheetlets. The dynamic rearrangement of E2A between diastole and systole has been demonstrated in healthy participants (Fig 1, *D*), whereas low E2A can be used to explain the mechanistic deficiencies in wall strain and to predict LV remodeling in participants with dilated cardiomyopathy (2). Studies exploring the regional impact of myocardial infarction on E2A and its relationship with long-term remodeling are lacking.

cDTI also allows for in vivo characterization of the helical arrangement of the myocardial fibers as demonstrated on dissection plates (14). The helix angle (HA) is a measure of the elevation angle of the primary eigenvector of the diffusion tensor, corresponding to the long-axis orientation of local cardiomyocytes, with respect to the short-axis plane (7). In healthy myocardium, HA progresses transmurally from myocytes with left-handed orientation at the epicardium, progressing through to myocytes with circumferential orientation in the mesocardium, to myocytes with right-handed orientation (RHM) at the endocardium (Fig 1, *C*). Wu et al (9) previously demonstrated infarct segments to exhibit a reduction in RHM after myocardial infarction, pointing to a loss of organization among subendocardial myocytes. Whereas the authors studied the relationship between HA and regional wall thickening, the predictive relevance of changes in HA for LV remodeling has not been fully elucidated.

To date, only a limited number of studies have performed cDTI on in vivo human hearts after myocardial infarction, mostly using stimulated echo acquisition mode cDTI (9). Single-shot spin-echo cDTI has been proposed as a refined alternative to stimulated echo acquisition mode, providing higher signal-to-noise ratio and more reproducible images (15). By allowing for free breathing and shorter scanning times (16), feasibility in patients who are acutely ill is enhanced.

We therefore performed second-order motion-compensated spin-echo cDTI in participants with reperfused ST-segment elevation myocardial infarction (STEMI) to assess acute and longitudinal changes of cDTI biomarkers after myocardial infarction with a particular focus on E2A and HA and to determine the association of acutely derived cDTI biomarkers with LV remodeling.

Materials and Methods

Participant Population

Patients who had a "first event" STEMI were prospectively recruited from a single tertiary center. Study inclusion criteria were as follows: *(a)* myocardial infarction as defined by current international guidelines (17), *(b)* revascularization by means of percutaneous coronary intervention within 12 hours after the onset of symptoms, and *(c)* no contraindications to cardiac MRI. Exclusion criteria were as follows: *(a)* previous revascularization procedure (coronary artery bypass grafts or percutaneous coronary intervention), *(b)* known cardiomyopathy, *(c)* severe valvular heart disease, *(d)* atrial fibrillation, and *(e)* hemodynamic instability lasting longer than 24 hours following percutaneous coronary intervention. The study protocol was approved by the institutional research ethics committee and complied with the Declaration of Helsinki. All participants gave written informed consent for their participation (National Institute of Health Research study no. 33963 and Research Ethics no. REC 17/YH/0062).

Cardiac MRI Protocol

The study protocol included a cardiac MRI examination within 3–7 days of index presentation (acute examination) and one at 3 months. Cardiac MRI examinations were performed with a 3.0-T scanner (Philips). The cardiac MRI protocol included full LV coverage with functional cine and late gadolinium enhancement (LGE) imaging, three matching short-axis sections (located at the base, mid, and apex) with cDTI, modified Look-Locker inversion (5[3]3) T1 mapping, T2 mapping, and postcontrast T1 mapping (see Appendix E1 [online] for pulse sequence parameters).

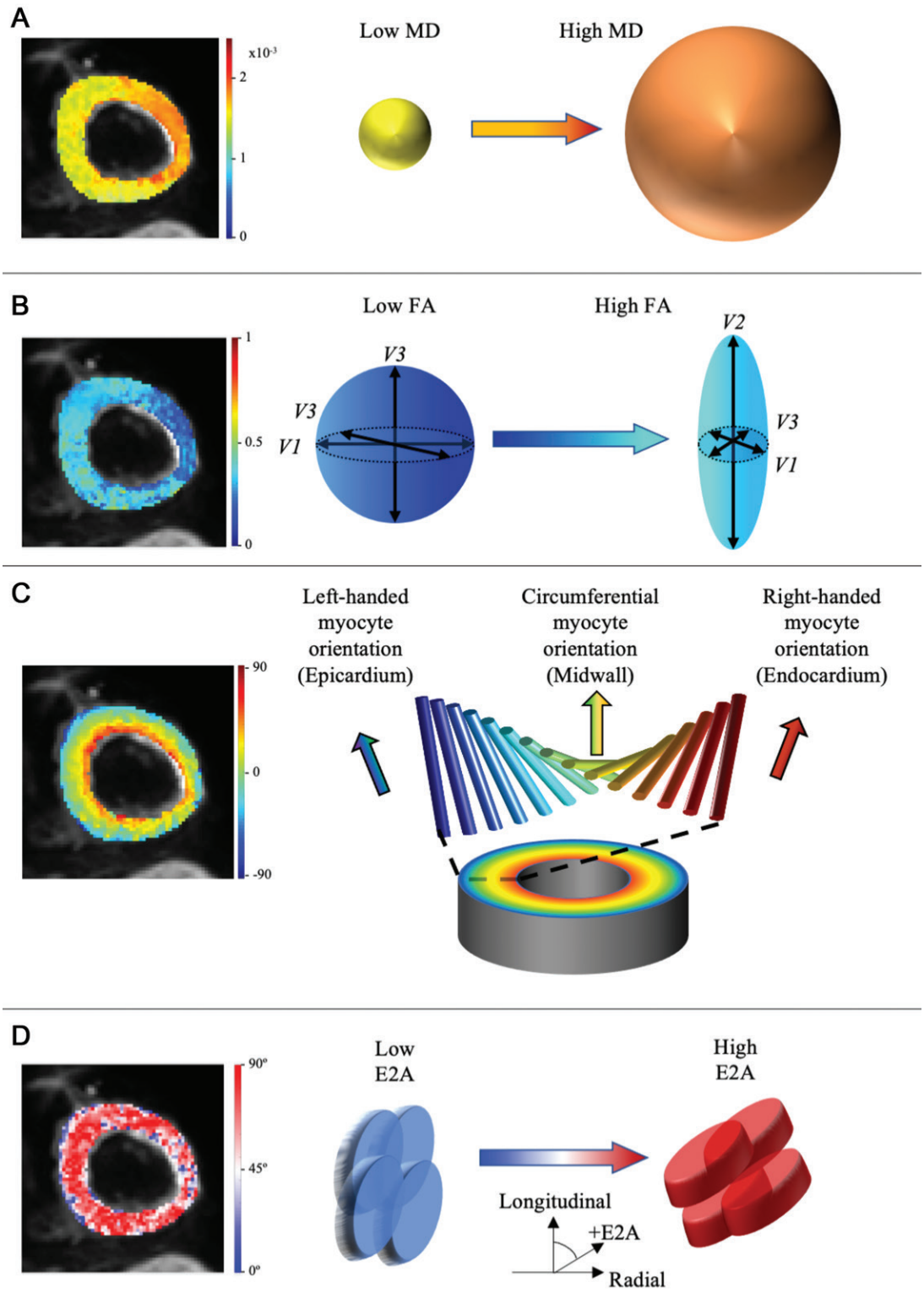

Figure 1: Diagram of diffusion tensor imaging markers. In healthy myocardium, cell membranes offer physiologic barriers to diffusion of water molecules and restrict diffusion to primarily the long axis (ie, *y*-axis) (V2) of myocytes. *A*, *B*, As cell membranes are destroyed, magnitude of diffusion increases. Hence, mean diffusivity (MD) increases (*A*), anisotropy of diffusion decreases (*B*), and fractional anisotropy (FA) decreases (*B*). V1 = x-axis, V3 = z-axis. *C*, Helix angle (HA) maps provide voxel-wise representation of average myocyte orientation. Histologic studies have shown subendocardial myocytes with right-handed orientation (RHM), midwall myocytes with circumferential orientation, and subepicardial myocytes with left-handed orientation (LHM). These orientation changes are quantified by HA measure, which ranges from −90° to 90° transmurally. Previous authors have measured proportions of HA voxels that belong to three categories of orientation—LHM (−90° ≤ HA < −30°), myocytes with circumferential orientation (−30° ≤ HA ≤30°), and RHM (30° < HA ≤90°). *D*, Secondary eigenvector angle (E2A) maps provide voxel-wise representation of angle of laminar sheetlets, which depicts the orientation of laminar sheetlets in midsystole.

cDTI Data

cDTI data were acquired using an electrocardiography-gated second-order motion-compensated single-shot spin-echo echo-planar imaging sequence with asymmetric bipolar diffusion waveforms (16) and respiratory navigator tracking with the following parameters: repetition time of three R-R intervals, echo time of 89 msec; flip angle, 90°; field of view, 238 × 238 mm; matrix, 108 × 105; acquired in-plane resolution, 2.20 × 2.27; section gap, 8 mm; reconstructed voxel size, 1.7 × 1.7 × 8 mm; sensitivity encoding acceleration, 1.8. Each cDTI data set constituted 18 noncollinear diffusion-weighted acquisitions with *b* values of 100 sec/mm^2 (three acquisitions), 200 sec/mm^2 (three acquisitions), and 500 sec/mm^2 (12 acquisitions). Based on cine data, trigger delay was set individually for each participant to coincide with 60% peak systole, and the center of k-space was approximately at 85% of peak systole.

Cardiac MRI Scan Analysis

Cine, mapping, and LGE data were analyzed with software (cvi42; Circle Cardiovascular Imaging) to derive left ventricular ejection fraction (LVEF) and tissue characteristics, including native T1 values, T2 values, extracellular volume (ECV), infarct size, and microvascular obstruction (MVO). cDTI data processing was performed with in-house–developed Matlab software (Mathworks) (Appendix E1 [online]). Tensor eigenvalues, MD, FA, HA, and E2A maps were calculated according to the tensors derived from diffusion-weighted imaging data acquired at diffusion gradients with images having *b* values of 100 sec/mm^2, 200 sec/mm^2, and 500 sec/mm^2. Endocardial and epicardial borders were manually delineated according to the reconstructed non–diffusion-weighted data. Both region of interest–based analysis and segmental analysis were performed as follows.

Region of interest analysis.—Regions of interest manually drawn in accordance with standards set by the European Association for Cardiovascular Imaging (18) were used for the analysis of T1, T2, ECV, MD, and FA. For each participant, three regions of interest were drawn corresponding to infarct (positive for LGE), adjacent edematous myocardium (negative LGE, raised native T1 [departmental threshold >1240 msec]), and remote myocardium (opposite infarct).

Segmental analysis.—After dividing each section into six equiangular segments starting from the anterior interventricular junction (19), segmental E2A and HA averages were derived. HA maps were described by classifying voxels into one of three groups—myocytes with left-handed orientation ($-90° \leq$ HA $< -30°$), myocytes with circumferential orientation ($-30° \leq$ HA $\leq 30°$), and RHM ($30° <$ HA $\leq 90°$)—and quantitative markers derived as the respective myocardial proportions of each type. To assess the interobserver reproducibility of diffusion tensor imaging analysis, all 30 acute cDTI scans were analyzed by a second experienced investigator (C.K., with 7 years of experience).

To investigate changes in cDTI parameters in participants with worsening LV function, three groups of participants were identified according to LVEF (in accordance with European Society of Cardiology Guidelines) (20), as follows: *(a)* group 1, with preserved LVEF (>50%); *(b)* group 2, with acutely impaired LVEF (<50%) that recovered to normal limits (>50%) by 3 months; and *(c)* group 3, with acutely impaired LVEF that remained impaired at 3 months (<50%).

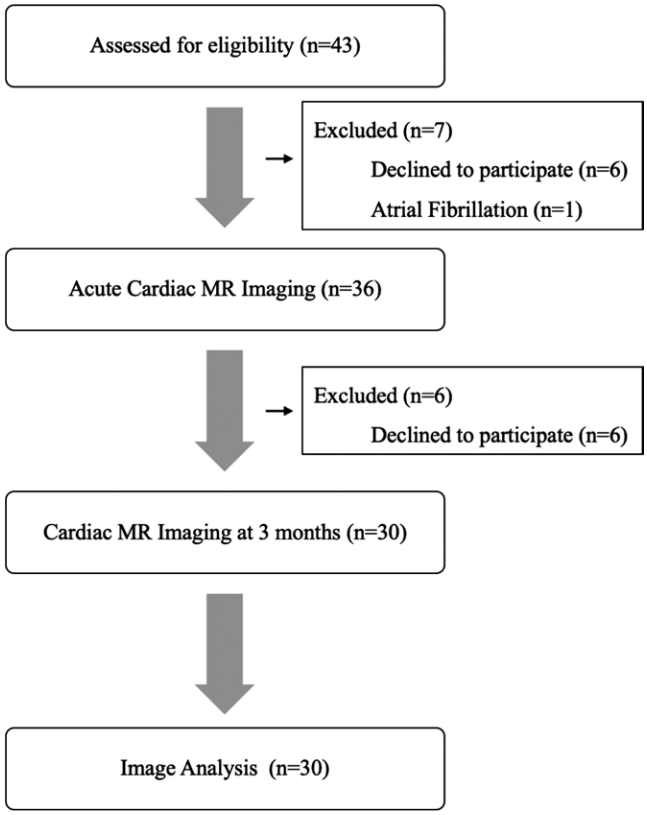

Figure 2: Flowchart of study enrollment.

Statistical Analysis

Statistical analyses were performed with IBM SPSS Statistics software (version 21.0). Normality was checked with the Shapiro-Wilk test. Continuous variables were reported as means ± standard deviations. Comparison between quantitative variables was performed with an independent-sample parametric statistical test (unpaired Student *t* test) or nonparametric statistical test (Mann-Whitney test) as appropriate. For comparing results from initial and repeated measurements, paired *t* tests and analysis of variance with Bonferroni posthoc comparisons were used. The Pearson correlation analysis was used to calculate the correlation coefficient among cDTI, T1, T2, and ECV values and with percentage of LVEF recovery. Univariable analyses were performed to identify predictors of reduced LVEF at 3 months. Variables with $P < .1$ in the univariable analysis were included in a multivariable linear regression analysis. Interobserver variability was analyzed using the Bland-Altman method. All tests were assumed to be statistically significant when $P < .05$.

Results

Baseline Participant Characteristics

The study flowchart is shown in Figure 2. Thirty participants (mean age ± standard deviation, 59 years ± 10; 21 men and

nine women) completed acute (mean, 5 days ± 2) and 3-month (mean, 104 days ± 14) examinations. As described in Table 1, 17 of 30 participants (56%) had inferior STEMI due to occlusion of the right coronary artery at presentation. At acute cardiac MRI examination, all participants showed evidence of edema on T2 maps and infarction on LGE images, with a mean infarct size of 10 g ± 8. By the 3-month cardiac MRI examination, the mean LVEF across the cohort improved from 48% ± 7 to 53% ± 7 (P = .006) (Table 2).

Table 1: Baseline Characteristics of Study Population

Participant Characteristic	Value (n = 30)
Age (y)*	59 ± 10
Sex (M/F)	21/9
Risk factors	
Smoker	11 (37)
Hypertension	4 (13)
Diabetes	2 (7)
Family history	9 (30)
Peripheral vascular disease	1 (3)
Characteristics at presentation	
Culprit coronary artery	
Left anterior descending artery	10 (33)
Left circumflex artery	3 (10)
Right coronary artery	17 (56)
Infarcted segments*†	4 ± 2
Microvascular obstruction	13 (43)
Time from onset of symptoms to balloon inflation (min)*	238 ± 172
Treatment	
Aspirin	30 (100)
Adenosine diphosphate receptor antagonist (Ticagrelor; AstraZeneca)	30 (100)
Angiotensin-converting enzyme inhibitor	30 (100)
Beta blocker	28 (93)

Note.—Except where indicated, data are number of participants, with percentages in parentheses.

* Numbers are means ± standard deviations.

† Established using segmental analysis on late gadolinium enhancement images.

cDTI Acquisition

cDTI acquisition was successful in all participants, with a mean acquisition time of 13 minutes ± 5. Representative cardiac MRI and cDTI maps are shown in Figure 3. Apical cDTI sections were excluded from analysis because of persistent artifacts from unsuppressed fat, signal loss, and suboptimal signal-to-noise ratio. Of all basal and middle section segments, 65 of 720 segments (9%) were excluded because of the mentioned image artifacts. Bland-Altman analysis of interobserver reproducibility is shown for MD (Fig E1, *A* [online]), FA (Fig E1, *B* [online]), E2A (Fig E1, *C* [online]), and HA (Fig E1, *D* and *E* [online]), demonstrating excellent interobserver agreement.

Table 2: Global Cardiac MRI Findings

Parameter	Acute Cardiac MRI Examination (n = 30)	3-month Cardiac MRI Examination (n = 30)
Interval from PCI to cardiac MRI examination (d)	5 ± 2	104 ± 14
LVEF (%)	48 ± 7	53 ± 7
LVEDV (mL)	154 ± 31	154 ± 34
LVEDVi (mL/m^2)	78 ± 15	78 ± 16
LVESV (mL)	75 ± 17	73 ± 24
LV mass (g)	105 ± 25	99 ± 23
Mean LGE (% of LV)	21 ± 14	15 ± 9
Infarct size (g)	10 ± 8	8 ± 6
No. of patients with MVO	13	0
MVO (g)	0.65 ± 1.18	Not applicable

Note.—Except where indicated, numbers are means ± standard deviations. LGE = late gadolinium enhancement, LVEDV = left ventricular end-diastolic volume, LVEDVi = left ventricular end-diastolic volume indexed for body surface area, LVEF = left ventricular ejection fraction, LVESV = left ventricular end-systolic volume, LV = left ventricle, MVO = microvascular obstruction, PCI = percutaneous coronary intervention.

cDTI Biomarkers after Acute Ischemic Injury

Acutely, MD and FA in remote myocardium matched previously reported values in healthy volunteers using single-shot spin-echo cDTI at 3 T (21). In keeping with previous literature, our results show MD to be increased in adjacent and infarct regions, with FA showing the opposite trend (Table 3).

Mean E2A values were lower in infarct segments compared to adjacent and remote segments (mean remote $E2A_c$ = 55° ± 9, mean adjacent E2A = 52° ± 7, mean infarcted E2A = 49° ± 10; analysis of variance P = .008) (Table 3). The HA range of infarct and remote segments during the acute cardiac MRI examination is shown in Figure 4, *A*. Infarct segments had less RHM compared to adjacent and remote segments (mean infarcted RHM = 9% ± 5, mean adjacent RHM = 20% ± 5, mean remote RHM = 16% ± 6; analysis of variance $P <$ .001). Proportions of RHM in infarcted segments as depicted on HA maps correlated with corresponding segmental E2A (Fig 4, *B*). Thirteen participants showed evidence of MVO on LGE images. Segmental E2A and percentage of RMH were lower in infarct segments with MVO compared with infarct

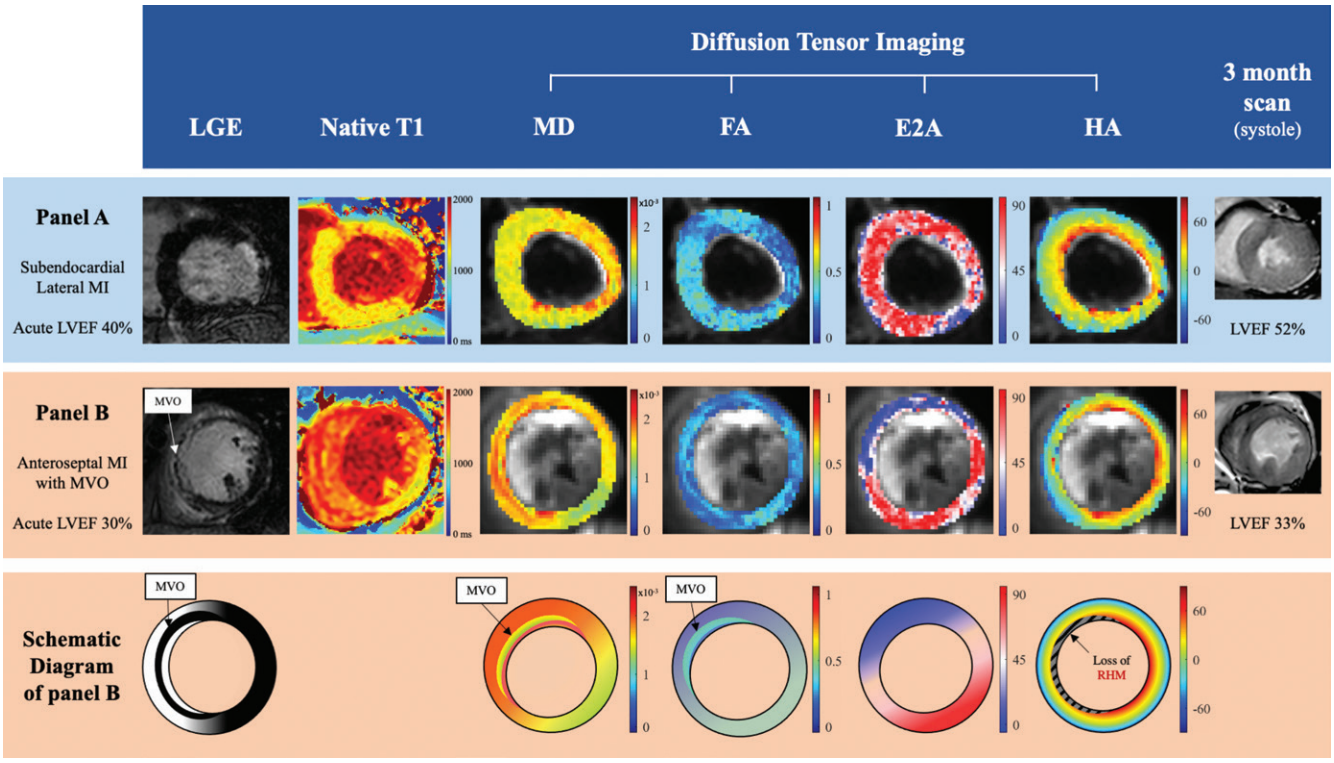

Figure 3: Representative cardiac MRI scans and cardiac diffusion tensor images. Panels *A* and *B* correspond to two separate participants. Panel *A*, Short-axis images in 61-year-old man 7 days after lateral ST-segment elevation myocardial infarction (STEMI) and subsequent primary percutaneous coronary intervention to obtuse marginal artery. His acute left ventricular ejection fraction (LVEF) was 40%. Late gadolinium enhancement (LGE) image demonstrates a subendocardial scar in basal anterolateral wall (column 1), with high T1 values on T1 map (column 2). Corresponding areas on cardiac diffusion tensor imaging (cDTI) maps show high mean diffusivity (MD) (column 3), low fractional anisotropy (FA) (column 4), high secondary eigenvector angle (E2A) (column 5), and preservation of myocytes with right-handed orientation (RHM) (red and orange pixels, 30°, helix angle [HA] ,90°) on HA maps. Participant's LVEF improved to 52% at 3 months. Panel *B*, Short-axis images in 61-year-old man 7 days after anteroseptal STEMI and subsequent primary percutaneous coronary intervention to left anterior descending artery. His LVEF was 30% at this stage. His LGE image demonstrates transmural scar and microvascular obstruction (MVO) in midseptal walls, with hyperintense signals on T1 map. Corresponding areas on cDTI maps show high MD and low FA. As demonstrated in schematic diagram, within infarct segments are areas of low MD and high FA, likely in relation to MVO artifact. Meanwhile, E2A maps show significantly low values, and HA shows less RHM (reduced red and orange pixels) in infarct segments compared with panel *A*. Participant's LVEF only improved to 33% at 3 months. MI = myocardial infarction.

segments without MVO both in acute (mean MVO E2A with ventricular ejection = 43° ± 4 vs mean MVO E2A without ventricular ejection = 50° ± 6, P = .031; mean MVO percentage of RHM with ventricular ejection = 5% ± 4 vs mean MVO percentage of RHM without ventricular ejection = 11% ± 5, $P < .001$) and 3-month cardiac MRI examination (mean MVO E2A with ventricular ejection = 40° ± 7 vs mean MVO E2A without ventricular ejection = 48° ± 9, P = .018; mean MVO percentage of RHM with ventricular ejection = 8% ± 5 vs mean MVO percentage of RHM without ventricular ejection = 13% ± 6, P = .008).

Longitudinal Changes in cDTI Biomarkers

Compared to the acute scans at 3 months, MD increased in infarct regions from 1.69 × 10^{-3} mm^2/sec ± 0.14 to 1.83 × 10^{-3} mm^2/sec ± 0.16 (Table 3). Conversely, FA decreased in the infarct regions from 0.25 ± 0.03 to 0.22 ± 0.03. MD and FA values in infarcted regions correlated with ECV at 3 months (Fig 5), indicating that in the absence of edema, both markers are sensitive to the expansion in ECV. There were no significant longitudinal changes in E2A or HA proportions, indicating that the microstructural changes they depict remain relatively fixed.

Predictive Value of Acute cDTI: Acute Biomarkers of Irreversible Injury and Long-term LV Dysfunction

Participants with lower acute FA in infarct regions experienced significantly less change in infarct size over time, whereas higher FA values were associated with significant reductions in final infarct size ($P < .001$) (Fig 6, *A*).

To understand the long-term implications of acute changes in cDTI parameters within infarct regions, we grouped participants according to LV recovery at 3 months (Table 4). Compared with participants with preserved LVEF at 3 months (groups 1 and 2), participants with impaired LVEF at 3 months (group 3) had significantly lower FA, lower RHM (Fig 6, *B*), and lower E2A in their infarct segments during the acute scan. Segmental RHM and E2A in acute infarct segments correlated with LVEF at 3 months (Fig 6, *C* and *D*). At 3 months, group 3 participants retained significantly lower E2A and percentage of RHM values in their infarct segments compared with infarct segments of participants in groups 1 and 2 (Table 4).

Univariable linear regression analysis (Table 5) identified several cardiac MRI-based infarct characteristics to be significantly associated with ejection fraction at 3 months. Among diffusion tensor imaging parameters, acute infarct FA, E2A, and RHM all correlated with LVEF at 3 months (r = 0.68, r = 0.59, and r = 0.53,

Table 3: Regional Cardiac MRI Findings

	Acute Scan (n = 30)				3-month Scan (n = 30)			
Parameter	Remote	Adjacent	Infarct	P Value	Remote	Adjacent	Infarct	P Value
T1 (msec)	1194 ± 66	1295 ± 75	1478 ± 123	<.001	1188 ± 42	1211 ± 62*	1398 ± 91*	<.001
ECV (%)	27 ± 3	32 ± 4	53 ± 9	<.001	29 ± 6	29 ± 6	60 ± 16*	<.001
T2 (msec)	50 ± 5	53 ± 6	68 ± 10	.009	48 ± 4	49 ± 5*	55 ± 5*	.007
MD ($\times 10^{-3}$ mm^2/sec)	1.48 ± 0.12	1.59 ± 0.10	1.69 ± 0.14	<.001	1.45 ± 0.11	1.53 ± 0.13*	1.83 ± 0.21*	<.001
FA	0.36 ± 0.02	0.33 ± 0.03	0.25 ± 0.03	<.001	0.35 ± 0.03	0.33 ± 0.02	0.22 ± 0.03*	.008
E2A (degrees)†	55 ± 9	52 ± 7	49 ± 10	.008	44 ± 11	51 ± 8	46 ± 9	.843
HA†								
RHM (%)	16 ± 6	20 ± 5	9 ± 5	<.001	19 ± 6	20 ± 6	12 ± 7	.343
CM (%)	78 ± 7	66 ± 11	80 ± 7	.617	68 ± 9	69 ± 11	77 ± 11	.786
LHM (%)	6 ± 5	14 ± 6	11 ± 9	.112	13 ± 7	11 ± 8	11 ± 8	.784

Note.—Except where indicated, numbers are means ± standard deviations. P values were obtained with analysis of variance. CM = myocytes with circumferential orientation, ECV = extracellular volume, E2A = secondary eigenvector angle, FA = fractional anisotropy, HA = helix angle, LHM = myocytes with left-handed orientation, MD = mean diffusivity, RHM = myocytes with right-handed orientation.

* Significant change from acute scan ($P < .05$).

† Measured with segmental analysis.

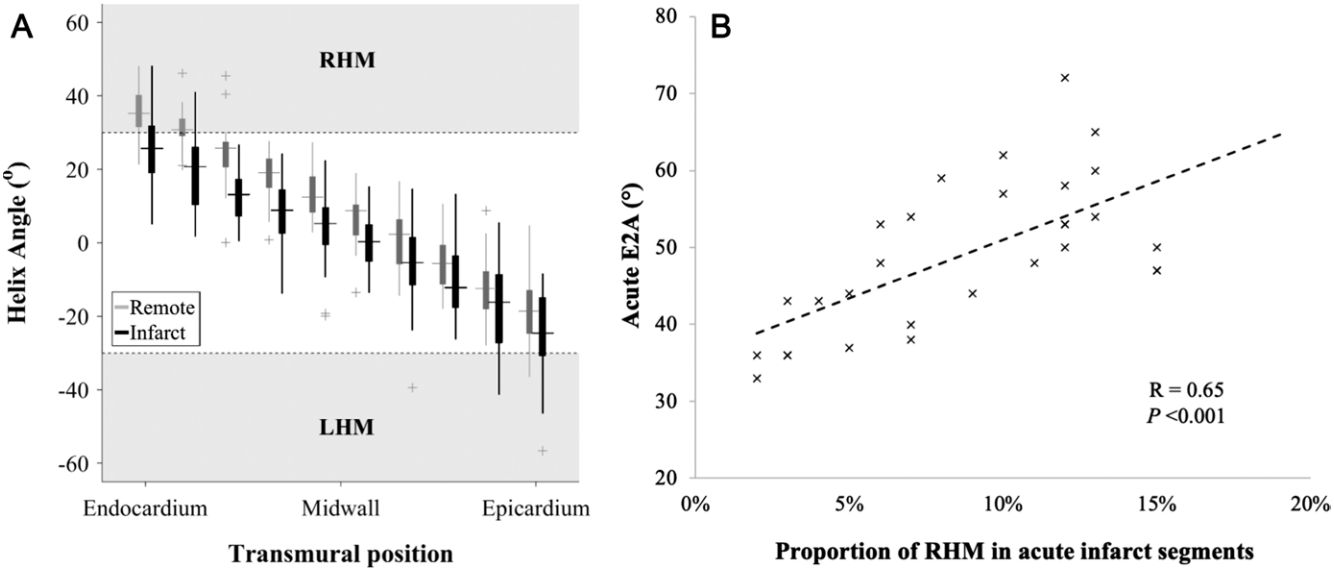

Figure 4: *A*, Plot of helix angle (HA) range transmurally across infarct and remote segments in acute scans, with infarct segments having less myocytes with right-handed orientation (RHM) than remote myocytes with left-handed orientation (LHM). *B*, Association between RHM and secondary eigenvector angle (E2A) values in corresponding infarct segments during acute scan.

respectively). In multivariable linear regression analysis adjusting for factors, including acute ejection fraction, infarct size and microvascular obstruction, only infarct FA (standardized β = 0.56, P = .008) was independently associated with LVEF at 3 months.

Discussion

Cardiac diffusion tensor imaging offers unique insights into in vivo microstructural changes following ST-segment elevation myocardial infarction. The main findings from this study are as follows: *(a)* myocardial sheetlets in acutely infarcted myocardium are unable to adopt their usual steep orientations in systole as suggested by low secondary eigenvector angle (E2A) values (mean remote E2A = 55° ± 9, mean infarcted E2A = 49° ± 10, $P < .001$); *(b)* the reduction of myocytes with right-handed orientation (RHM) on helix angle (HA) maps is likely reflective of a loss of organization among subendocardial myocytes (mean remote RHM = 16% ± 6, mean infarcted RHM = 9% ± 5, $P < .001$) (22); *(c)* whereas longitudinal changes in mean diffusivity (MD) and fractional anisotropy (FA) suggest diffusion becomes more unrestricted and isotropic (mean infarcted MD = 1.83 × 14^{-3} mm^2/sec ± 0.21, mean infarcted FA = 0.22 ± 0.03), eigenvector-related parameters, such as E2A and HA proportions, do not change longitudinally, which suggests that the axes of microstructural organization remain relatively fixed after injury; and *(d)* acute FA (r = 0.68, $P <$ .001), E2A (r = 0.59, $P < .001$), and RHM (r = 0.53, $P <$

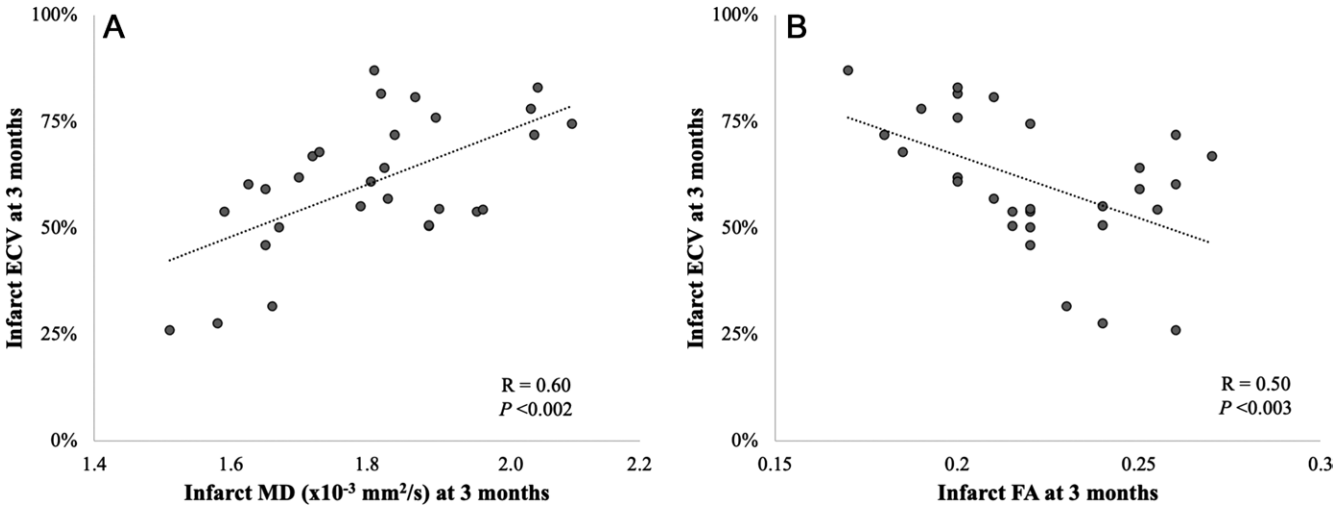

Figure 5: Graphs show correlation between extracellular volume (ECV) and, *A*, mean diffusivity (MD) and, *B*, fractional anisotropy (FA) at 3 months. MD and FA both correlate with ECV values in corresponding infarct regions.

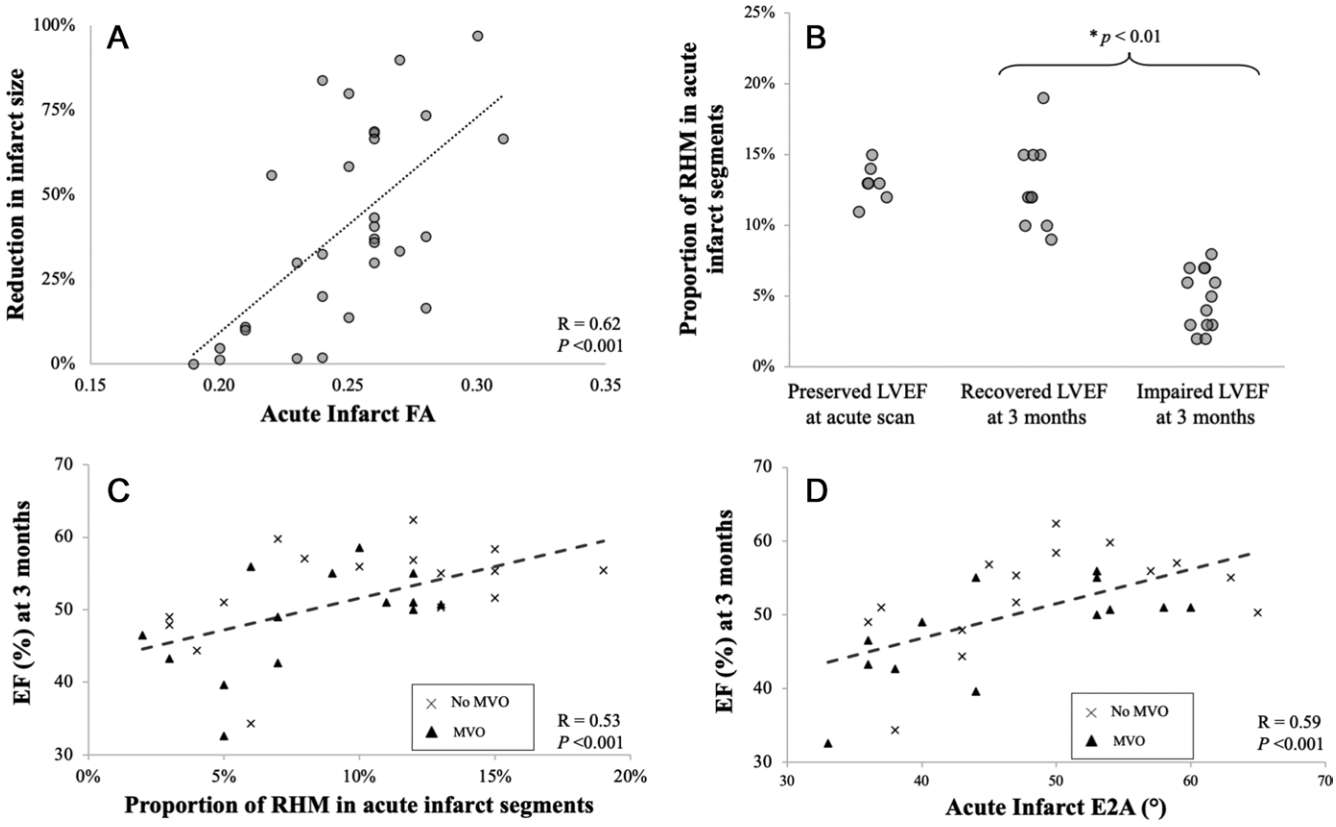

Figure 6: Graphs show correlation between acute diffusion tensor imaging parameters, infarct size, and percentage of left ventricular ejection fraction (LVEF) at 3 months. *A*, Participants with lower mean fractional anisotropy (FA) values in infarct regions had significantly less change in their infarct size between acute and 3-month scans. *B*, Participants with impaired LVEF at 3 months had significantly lower proportions of myocytes with right-handed orientation (RHM) in their infarct segments in their acute scans. *C*, *D*, Lower proportions of, *C*, RHM and, *D*, segmental secondary eigenvector angle (E2A) in acute infarct segments correlated with lower percentage of LVEF at 3 months. EF = ejection fraction, MVO = microvascular obstruction.

.001) within infarct segments all correlate with left ventricular ejection fraction (LVEF) at 3 months and after multivariable regression analysis. Having lower FA values within acutely infarcted myocardium was independently predictive of poor percentage of LVEF recovery (standardized β = 0.57, *P* = .008). These findings help elucidate the microstructural effects of acute myocardial infarction and may provide novel acute biomarkers for risk stratification.

Congruent with the theory of the ischemic wave-front phenomenon (23), large circumferentially oriented collagen fibers deposit first in the damaged subendocardium (22). Wu et al (9) demonstrated significant reductions of RHM in infarct

Table 4: cDTI Characteristics of Participants with Different LVEF Outcomes after STEMI

Characteristic	Group 1 (n = 7)	Group 2 (n = 10)	Group 3 (n = 13)	P Value
Acute scan				
LVEDV (mL)	140 ± 22	149 ± 28	152 ± 34	.653
LVEF (%)	53 ± 2	44 ± 3	41 ± 5	.002
Infarct size (g)	7 ± 6	11 ± 6	15 ± 9	<.001
MVO (g)	0	0.12 ± 0.38	1.1 ± 1.5	.012
Infarct T1 (msec)	1380 ± 136	1468 ± 101	1532 ± 84	.049
Infarct ECV (%)	48 ± 7	54 ± 11	54 ± 5	.034
Infarct MD ($\times 10^{-3}$ mm^2/sec)	1.69 ± 0.05	1.66 ± 0.07	1.75 ± 0.1	.022
Infarct FA	0.27 ± 0.03	0.26 ± 0.02	0.23 ± 0.03	.004
Infarct E2A (degrees)	56 ± 9	52 ± 7	40 ± 5	.005
Infarct RHM (%)	12 ± 2	11 ± 3	4 ± 2	<.001
3-month scan				
LVEDV (mL)	135 ± 22	158 ± 34	171 ± 41	.074
LVEF (%)	55 ± 4	56 ± 3	43 ± 5	<.001
Infarct size (g)	3.6 ± 6	6.4 ± 4	11.4 ± 7	<.001
Infarct T1 (msec)	1363 ± 96	1395 ± 62	1442 ± 88	.240
Infarct ECV (%)	58 ± 12	54 ± 19	64 ± 12	.945
Infarct MD ($\times 10^{-3}$ mm^2/sec)	1.78 ± 0.17	1.81 ± 0.12	1.88 ± 0.14	.336
Infarct FA	0.23 ± 0.04	0.22 ± 0.03	0.21 ± 0.02	.587
Infarct E2A (degrees)	48 ± 7	50 ± 6	39 ± 8	.007
Infarct RHM (%)	15 ± 6	16 ± 6	5 ± 2	.009

Note.—Except where indicated, number are means ± standard deviations. Group 1 had preserved left ventricular ejection fraction (LVEF) at the acute scan, Group 2 had recovered LVEF at 3 months, and Group 3 had impaired LVEF at 3 months. P values were obtained with analysis of variance. cDTI = cardiac diffusion tensor imaging, ECV = extracellular volume, E2A = secondary eigenvector angle, FA = fractional anisotropy, HA = helix angle, LVEDV = left ventricular end-diastolic volume, MD = mean diffusivity, MVO = microvascular obstruction, RHM = myocytes with right-handed orientation, STEMI = ST-segment elevation myocardial infarction.

segments 26 days after myocardial infarction. Our results demonstrate this reduction can be detected in as early as 5 days, but this could be reflective of a combination of factors, including: *(a)* discontinuity in myocyte trajectory because of ischemic loss of subendocardial myocardium with deposition of collagen fibers more circumferentially oriented (24) and *(b)* possible reorientation of cardiomyocytes because of the deforming effect of adjacent noninfarcted myocardium in the longitudinal and radial directions (22). Our results are corroborated by findings of concomitant reduced E2A in segments with reduced RHM, suggesting that disruption of the subendocardial myocyte organization affects the ability of the myocardial sheetlets to adopt their usual steep orientations in systole (2,22). This is particularly apparent in segments with MVO. Meanwhile, participants with a higher percentage of RHM and E2A values in their acute infarct segments had a higher percentage of LVEF at 3 months.

In a recent study by Moulin et al (13), the authors demonstrated the superior diagnostic ability of MD maps in depicting acute myocardial edema compared with T1 and T2 maps, indicating that interstitial edema contributes substantially to the acute changes in MD after ischemic injury. This, however, makes it highly challenging to ascertain how much irreversible injury has occurred from MD alone in the presence of edema. FA values reflect the anisotropy of diffusion, and studies have shown FA values to correlate negatively with histologic measurements of collagen, a major component of fibrotic tissue (10). In the early stages after myocardial infarction, reductions in FA within infarct segments could be representative of edema and the accumulation of spherical inflammatory cells, such as swollen myocytes and myofibroblasts, as shown in previous histologic studies (6,25). As the edema settles over time and necrotic myocytes are replaced by collagen fibers, the further longitudinal reductions in FA in our results are likely reflective of the deposition of collagen and the disarray of fibers (10,22). Longitudinal changes in MD and FA in our results correlate with the increase in ECV and highlight the dynamic nature of changes taking place within infarct zones. Despite this serial change over 3 months, participants with lower infarct FA values in the acute scan had significantly less change in infarct size over time and worse LV function at 3 months. Hence, unlike MD, FA is potentially capable of detecting irreversible injury even in the acute stages in the presence of edema.

Contrary to MD and FA, eigenvector-related biomarkers like HA and E2A undergo little change overtime, suggesting that changes to the axes of microstructural components can be detected in the acute stages of myocardial infarction and remain relatively fixed. Hence, they are ideally suited for predicting LV remodeling, and this presents a potential clinical use of cDTI in the realms of acute imaging after myocardial infarction; however, a more comprehensive understanding is still required regarding the effects of edema and MVO on E2A and HA.

Recruiting participants after STEMI for complex acute and longitudinal imaging was challenging, and the study sample size was therefore relatively small but aligned with similar studies

Table 5: Predictors of Decreased Ejection Fraction in Univariable and Multivariable Regression Analysis

Cardiac MRI Characteristic on Acute Scan	Univariable Analysis		Multivariable Analysis	
	r	*P* Value	β	*P* Value
LVEF (%)	0.49	.006	−0.14	.582
Infarct size (g)	−0.50	.005	−0.18	.464
MVO size (g)	−0.42	.020	−0.07	.698
Infarct T1 (msec)	−0.39	.079	…	…
Infarct T2 (msec)	0.26	.339	…	…
Infarct ECV (%)	−0.47	.022	−0.18	.334
Infarct MD ($\times 10^{-3}$ mm^2/sec)	−0.05	.411	…	…
Infarct FA	0.68	<.001	0.56	.008
Infarct E2A (degrees)	0.59	<.001	0.18	.391
Infarct RHM (%)	0.53	<.001	0.23	.284
Infarct CM (%)	0.20	.294	…	…
Infarct LHM (%)	0.42	.210	…	…

Note.—Variables are taken from the acute scan. Multivariable standardized regression coefficient (β) and *P* values are shown where the variable was included in the multivariable analysis. CM = myocytes with circumferential orientation, ECV = extracellular volume, E2A = secondary eigenvector angle, FA = fractional anisotropy, HA = helix angle, LHM = myocytes with left-handed orientation, LVEF = left ventricular ejection fraction, MD = mean diffusivity, MVO = microvascular obstruction, RHM = myocytes with right-handed orientation.

(9). Conclusions drawn from this study were based on correlations with published evidence and other cardiac MRI markers, whereas validation with histologic specimens would be preferable. By allowing for unenhanced and free-breathing scans, single-shot spin-echo cDTI offers some practical benefits in the context of acute imaging after STEMI. However, acquisition was limited to only three sections, and technical developments are needed to allow for full LV coverage in shorter scanning times. Postprocessing can be labor intensive, and clinical implementation requires further optimization, particularly with tractography postprocessing for accurate definition of HA variation across the myocardium and scar borders (12).

In conclusion, our study demonstrated the unique capabilities of cardiac diffusion tensor imaging (cDTI) in helping assess microstructural changes after ST-segment elevation myocardial infarction, which can help elucidate the underlying pathophysiologic process of left ventricular remodeling. Despite the microstructural remodeling that is known to occur within scar tissue, helix angle and secondary eigenvector angle maps are able to depict early changes to the axes of microstructural components, which remain fixed over time and correlate with left ventricular ejection fraction (LVEF) at 3 months. Furthermore, low fractional anisotropy values in acutely infarcted myocardium are suggestive of severe injury and are independently predictive of poor LVEF recovery. Whereas clinical applications of cDTI are yet to be fully validated and established, our findings highlighted the potential clinical use of acutely derived cDTI biomarkers after myocardial infarction for predicting long-term adverse remodeling.

Acknowledgments: The authors thank the clinical staff of the cardiac MRI department at Leeds General Infirmary and the research nurses of Leeds Institute of Cardiovascular and Metabolic Medicine, University of Leeds, for their assistance in recruiting, scanning, and collecting data for this study.

Author contributions: Guarantors of integrity of entire study, A.D., E.D.; study concepts/study design or data acquisition or data analysis/interpretation, E.D., A.D., C.K.; manuscript drafting or manuscript revision for important intellectual content, A.D., E.D.; approval of final version of submitted manuscript, all authors; agrees to ensure any questions related to the work are appropriately resolved, all authors; literature research, A.D., E.D.; clinical studies, A.D., E.D., I.T., A.C., T.P.C.; experimental studies, C.K., I.T., C.T.S.; statistical analysis, A.D., E.D.; and manuscript editing, A.D., C.K., I.T., C.T.S., S.K., L.A.E.B., C.E.D.S., T.P.C., P.G.C., P.P.S., E.L., J.P.G., J.E.S., S.P., E.D.

Disclosures of Conflicts of Interest: **A.D.** Activities related to the present article: receives payment for provision of equipment or administrative support from British Heart Foundation; is employed with Heart Research UK. Activities not related to the present article: disclosed no relevant relationships. Other relationships: disclosed no relevant relationships. **C.K.** disclosed no relevant relationships. **I.T.** disclosed no relevant relationships. **C.T.S.** disclosed no relevant relationships. **S.K.** disclosed no relevant relationships. **A.C.** disclosed no relevant relationships. **L.A.E.B.** disclosed no relevant relationships. **C.E.D.S.** disclosed no relevant relationships. **T.P.C.** disclosed no relevant relationships. **P.G.C.** disclosed no relevant relationships. **N.J.** disclosed no relevant relationships. **P.P.S.** disclosed no relevant relationships. **E.L.** disclosed no relevant relationships. **J.P.G.** Activities related to the present article: institution received a grant from British Heart Foundation. Activities not related to the present article: disclosed no relevant relationships. Other relationships: disclosed no relevant relationships. **J.E.S.** disclosed no relevant relationships. **S.P.** Activities related to the present article: institution a received grant from British Heart Foundation. Activities not related to the present article: disclosed no relevant relationships. Other relationships: disclosed no relevant relationships. **E.D.** Activities related to the present article: institution received grants from British Heart Foundation and Heart Research UK; institution receives financial support from British Heart Foundation for travel to meetings for the study or other purposes; institution receives payment from British Heart Foundation for provision of writing assistance, medicines, equipment, or administrative support. Activities not related to the present article: receives payment for lectures, including service on speakers bureaus. Other relationships: disclosed no relevant relationships.

References

1. Gerdes AM, Capasso JM. Structural remodeling and mechanical dysfunction of cardiac myocytes in heart failure. J Mol Cell Cardiol 1995;27(3):849–856.
2. Nielles-Vallespin S, Khalique Z, Ferreira PF, et al. Assessment of Myocardial Microstructural Dynamics by In Vivo Diffusion Tensor Cardiac Magnetic Resonance. J Am Coll Cardiol 2017;69(6):661–676.
3. Nielles-Vallespin S, Scott A, Ferreira P, Khalique Z, Pennell D, Firmin D. Cardiac Diffusion: Technique and Practical Applications. J Magn Reson Imaging 2020;52(2):348–368.
4. Lee SE, Nguyen C, Yoon J, et al. Three-dimensional Cardiomyocytes Structure Revealed By Diffusion Tensor Imaging and Its Validation Using a Tissue-Clearing Technique. Sci Rep 2018;8(1):6640.
5. Holmes AA, Scollan DF, Winslow RL. Direct histological validation of diffusion tensor MRI in formaldehyde-fixed myocardium. Magn Reson Med 2000;44(1):157–161.
6. Chen J, Song SK, Liu W, et al. Remodeling of cardiac fiber structure after infarction in rats quantified with diffusion tensor MRI. Am J Physiol Heart Circ Physiol 2003;285(3):H946–H954.
7. Teh I, McClymont D, Burton RAB, et al. Resolving fine cardiac structures in rats with high-resolution diffusion tensor imaging. Sci Rep 2016;6(1):30573.
8. Nguyen C, Fan Z, Xie Y, et al. In vivo contrast free chronic myocardial infarction characterization using diffusion-weighted cardiovascular magnetic resonance. J Cardiovasc Magn Reson 2014;16(1):68.
9. Wu MT, Su MYM, Huang YL, et al. Sequential changes of myocardial microstructure in patients postmyocardial infarction by diffusion-tensor cardiac MR: correlation with left ventricular structure and function. Circ Cardiovasc Imaging 2009;2(1):32–40, 6, 40.

10. Abdullah OM, Drakos SG, Diakos NA, et al. Characterization of diffuse fibrosis in the failing human heart via diffusion tensor imaging and quantitative histological validation. NMR Biomed 2014;27(11):1378–1386.
11. Ariga R, Tunnicliffe EM, Manohar SG, et al. Identification of Myocardial Disarray in Patients With Hypertrophic Cardiomyopathy and Ventricular Arrhythmias. J Am Coll Cardiol 2019;73(20):2493–2502.
12. Mekkaoui C, Jackowski MP, Kostis WJ, et al. Myocardial scar delineation using diffusion tensor magnetic resonance tractography. J Am Heart Assoc 2018;7(3):e007834.
13. Moulin K, Viallon M, Romero W, et al. MRI of reperfused acute myocardial infarction edema: ADC quantification versus T1 and T2 mapping. Radiology 2020;295(3):542–549.
14. Scollan DF, Holmes A, Winslow R, Forder J. Histological validation of myocardial microstructure obtained from diffusion tensor magnetic resonance imaging. Am J Physiol 1998;275(6):H2308–H2318.
15. von Deuster C, Stoeck CT, Genet M, Atkinson D, Kozerke S. Spin echo versus stimulated echo diffusion tensor imaging of the in vivo human heart. Magn Reson Med 2016;76(3):862–872.
16. Stoeck CT, von Deuster C, Genet M, Atkinson D, Kozerke S. Second-order motion-compensated spin echo diffusion tensor imaging of the human heart. Magn Reson Med 2016;75(4):1669–1676.
17. Fihn SD, Blankenship JC, Alexander KP, et al. 2014 ACC/AHA/AATS/PCNA/SCAI/STS focused update of the guideline for the diagnosis and management of patients with stable ischemic heart disease: a report of the American College of Cardiology/American Heart Association Task Force on Practice Guidelines, and the American Association for Thoracic Surgery, Preventive Cardiovascular Nurses Association, Society for Cardiovascular Angiography and Interventions, and Society of Thoracic Surgeons. Circulation 2014;130(19):1749–1767.
18. Messroghli DR, Moon JC, Ferreira VM, et al. Clinical recommendations for cardiovascular magnetic resonance mapping of T1, T2, T2* and extracellular volume: A consensus statement by the Society for Cardiovascular Magnetic Resonance (SCMR) endorsed by the European Association for Cardiovascular Imaging (EACVI). J Cardiovasc Magn Reson 2017;19(1):75 [Published correction appears in J Cardiovasc Magn Reson 2018;20(1):9.].
19. Cerqueira MD, Weissman NJ, Dilsizian V, et al. Standardized myocardial segmentation and nomenclature for tomographic imaging of the heart. A statement for healthcare professionals from the Cardiac Imaging Committee of the Council on Clinical Cardiology of the American Heart Association. Circulation 2002;105(4):539–542.
20. Ponikowski P, Voors AA, Anker SD, et al. 2016 ESC guidelines for the diagnosis and treatment of acute and chronic heart failure [in Russian]. Russ J Cardiol 2017;1(141):7–81.
21. Scott AD, Nielles-Vallespin S, Ferreira PF, et al. An in-vivo comparison of stimulated-echo and motion compensated spin-echo sequences for 3 T diffusion tensor cardiovascular magnetic resonance at multiple cardiac phases. J Cardiovasc Magn Reson 2018;20(1):1.
22. Holmes JW, Nuñez JA, Covell JW. Functional implications of myocardial scar structure. Am J Physiol 1997;272(5 Pt 2):H2123–H2130.
23. Reimer KA, Jennings RB. The "wavefront phenomenon" of myocardial ischemic cell death. II. Transmural progression of necrosis within the framework of ischemic bed size (myocardium at risk) and collateral flow. Lab Invest 1979;40(6):633–644.
24. Mojsejenko D, McGarvey JR, Dorsey SM, et al. Estimating passive mechanical properties in a myocardial infarction using MRI and finite element simulations. Biomech Model Mechanobiol 2015;14(3):633–647.
25. Wang Y, Cai W, Wang L, et al. Evaluation of the differences of myocardial fibers between acute and chronic myocardial infarction: Application of diffusion tensor magnetic resonance imaging in a rhesus monkey model. Korean J Radiol 2016;17(5):725–733.